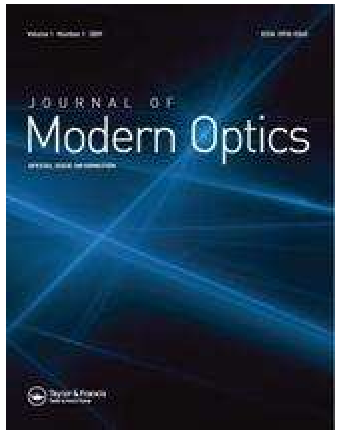

Ray tracing and scalar diffraction calculations of wavefronts, caustics and complex amplitudes in optical systems

Journal:	*Journal of Modern Optics*
Manuscript ID:	Draft
Manuscript Type:	Regular Paper
Date Submitted by the Author:	n/a
Complete List of Authors:	bosch, salvador; universitat de barcelona
Keywords:	wavefronts, caustics, image formation, scalar diffraction

Ray tracing and scalar diffraction calculations of wavefronts, caustics and complex amplitudes in optical systems

Salvador Bosch

Dept. Física Aplicada i Optica, Universitat de Barcelona, Diagonal 647, 08028 Barcelona, Spain

sbosch@ub.edu

Ray tracing and scalar diffraction calculations of wavefronts, caustics and complex amplitudes in optical systems

The procedures for precise calculation of wavefronts, caustics and complex amplitudes in optical systems are developed. Numerical methods are compared with analytical formulae for caustics. The conditions for the validity of the integration on wavefronts for obtaining the complex amplitudes (and hence intensities defining the PSFs) within scalar diffraction theory are discussed in detail. To illustrate the precision of the results obtained with the developed techniques, an experiment showing quite unexpected results is studied and explained in detail.

Keywords: wavefronts; caustics; image formation; scalar diffraction

1. Introduction

Ray tracing is the basis for the practical study of optical systems and most of the optical design procedures are completely based on that method. However, it is not a standard practice to use ray tracing for calculating and plotting wavefronts and caustics. Regarding calculations in image formation, it is well known that the point spread function (PSF) cannot be calculated from ray tracing and the scalar diffraction theory is used instead in instrumental optics. Our aim is to develop ray tracing procedures for illustrating several basic concepts related to aberration theory, wavefronts and caustics. Subsequently, by combining these geometrical results with those of scalar diffraction theory, very precise computations in instrumental optics will be implemented. Some significant experimental examples will be presented to illustrate the practical relevance of our procedures.

The paper is organized as follows. In Section 2, the procedures for calculating wavefronts and caustics on the basis of ray tracing techniques are presented. In Section 3, scalar diffraction theory is used for the precise calculation of the PSF; the accuracy and self consistency of those calculations is analyzed in Section 4. Section 5 presents a practical striking example that illustrates the interest and accuracy of the present work. An overall summary is presented in Section 6.

2. Raytracing, wavefronts and caustics

2.1. Calculating wavefronts.

Ray tracing is the most basic tool for the analysis of optical systems. Wavefronts can be calculated basing on the same principles as ray tracing, but it is not common practice to use wavefronts for the study of optical systems. In the present paper, we will limit our analysis to optical systems with full rotational symmetry, for simplicity. This implies that we restrict our object to be on axis and, consequently, the aberrations will be restricted to combinations of spherical and defocus. Under these circumstances our results will be, strictly speaking, quite restrictive in practical situations, but will serve to illustrate the concepts in full, with the simplicity obtained by the validity of a 2-D geometrical scheme: all our results can be represented using the meridian plane only. Within this scheme, in the geometrical sense, caustics are simply the envelope of the family of rays in the image zone as these rays smoothly increase the angle with respect to the axis. It is not immediately evident how to numerically calculate a caustic. A quite intuitive procedure can be established as follows, starting with the determination of wavefronts.

Consider our optical system consisting of a real axial point object O and a single converging lens where the object distance is greater than the focal length, so that rays will exit the lens converging towards the focal zone. Under these circumstances, the spherical aberration fully describes the behavior of the rays [1]. Let us now explain how to plot the wavefront in the image space which contains the axial point P_0, which is at a distance z from the concave vertex of a meniscus lens (see Fig. 1). Since the wavefront is the surface containing the points where the optical path travelled by light coming from the object is a fixed quantity, by considering precisely the axial ray ($h=0$) we conclude that the optical path corresponding to that wavefront is

$$C(z) = d + n \times d_0 + z \qquad (1)$$

where d is the distance from the object O to the convex vertex, d_0 the thickness of the lens and n its refractive index. Thus, a simple graphical procedure for plotting the profile of the wavefront corresponding to any distance z consists of

1) calculating $C(z)$.

2) sending rays from the object to the lens at increasing heights h, making them to refract at the two sides of the lens (while accumulating the value of the traveled optical path) and propagating the resulting rays into the image space only for the exact distance that makes all the optical paths to be exactly equal to $C(z)$.

Thus, the graphical procedure is simple and has general validity, i.e., could be equally used without the restrictions about rotational symmetry of the system that we are assuming here to keep the 2-D scheme. The method will determine the points P_h, as illustrated in Fig. 1. Note that, in our case it is only necessary to consider $h>0$ due to the mentioned rotational symmetry.

Eventually, for each plane z and taking h as parameter, the wavefront is mathematically defined by

$$\begin{cases} x(z;h) \\ y(z;h) \end{cases} \qquad (2)$$

Note that we name these two components that parametrically define the curve with respect to h for each z by means of the usual (X,Y) cartesian designation corresponding to the horizontal and vertical directions. Thus, $x(z;h)$ is simply the difference between the longitudinal (along the optical axis) coordinates of the points P_h and P_0 and $y(z;h)$ is the distance between P_h and the optical axis.

In all the following, to be specific, we will illustrate our procedures with an optical system consisting of a meniscus lens with radii 59.0 mm and 128.9 mm, refractive index 1.5151 (for wavelength 633 nm), center thickness $d_0 = 5.4\,mm$ and working with axial object distant d=419.9 mm from the convex side of the lens. Then, the Gaussian image plane (containing the center of the reference sphere) is at 400.0 mm from the concave side of the lens.

At this point we are already in position of performing a good and convenient checking for the numerical procedures just exposed. We may ask ourselves how well our numerical-graphical procedure compares with the well known analytical expressions for the wavefront aberration, in the particular case of our single lens. For example, in case of spherical aberration the analytical expression for the deviation between the real wavefront and the reference sphere has a dependence in the 4th power with respect to the height h up to the maximum value defining the pupil h_p, which corresponds to a radius r_p of the exit pupil [1]. In other words, the aberration is $A_e\rho^4$, where A_e is the peak spherical aberration coefficient and ρ the normalized pupil coordinate ($\rho = \frac{r}{r_p}, \quad 0 \le \rho \le 1$) and the only relevant quantity that defines the differences between the ideal and aberrated wavefront is the mentioned peak value A_e. Stated in another way: aberration theory tells us that we can quantify the nature and amount of aberration within the pupil by simply tracing a ray through the border and computing a difference in optical paths. Thus, what we are going to check numerically is, in fact, the practical validity of all these equivalent assumptions.

In our present case, the radius of the reference sphere passing through the concave vertex of the lens is greater than the radius of the concave side of the lens. Then, to avoid virtual paths in our previous procedures, we have performed the calculations for z=5.0 mm. We have checked that, up to h_p=22.0 mm, the numerically calculated quantity $x(5.0;h)$ corresponding to points P_h lays in front of the reference sphere (centered at at 400.0 mm from the concave side of the lens and passing through the point z=5.0 mm) by an amount $A_e\rho^4$ with $A_e = 88.6\lambda$ with an accuracy of a fraction of the wavelength for $0 \le \rho \le 1$ In terms of aberration theory language one says, simply, that there are 88.6 wavelengths of spherical aberration. Note that the required accuracy has to be always a quantity small with respect to the wavelength.

2.2 Calculating caustics

An interesting phenomenon may be easily visualized when the previous procedure is performed for values *z* closer to the paraxial (Gaussian) image plane of our point object, as illustrated in Fig. 2 for *z*=250 mm, with $0 \le h \le 28.0$ mm. Under these circumstances, the wavefront becomes a complex-shaped surface, as the function $y(z;h)$ (and also the function $x(z;h)$) becomes non-monotonic with respect to *h*. This is the key fact that defines the position of the caustic for any plane *z*: as we increase the height *h* of our ray, it seems natural that the values $y(z;h)$ tend also to increase, but there is a point at the wavefront where the function $y(z;h)$ becomes non-monotonic with respect to h and this is the wavefront caustic In fact, the function $x(z;h)$ becomes non-monotonic with respect to h as well.

It is important to understand how the wavefront is being obtained in Fig. 2. We send rays with increasing h value to the lens (in this figure the increment is Δh=0.28 mm) and by means of a ray tracing procedure up to a fixed accumulated optical path, the points P_h of the wavefront (see Fig. 1) are being plotted as dots in Fig. 2. These points P_h in Fig. 2 start from (0,0), which corresponds to P_0. When increasing h , for a certain height h_c one gets a cusp along the line: the turning point of the dots (here around 5.35 mm height) corresponding to h_c~21.5 mm For higher heights $h > h_c$ of the incoming ray, the wavefront folds. Thus, one may say that the wavefront is well defined (not ambiguously) for the optical path $C(z)$ provided the lens aperture is being limited to ray heights kept less than h_c. If rays enter the lens above that height, the wavefront at plane z is not well defined, since there will be two rays (thus two values of the optical path) reaching the same height of the plane.

From differential geometry, in the particular case where only spherical aberration is present, it is simple to find the analytical expression for the meridian section of the caustic. In fact the mathematical theory demonstrates that there are two sheets, being one coincident with the optical axis. The detailed calculation for the other sheet of the caustic (outer from the optical axis) is done in Chapter 7 of Ref. [1], and we simply use the formulae presented there. Accordingly, if we consider a cartesian coordinate system with origin at the exit pupil and independent variable Z, the equation for the upper part of the outer sheet of the caustic is

$$y = \frac{1}{3^{\frac{3}{2}}\sqrt{\frac{R.A_e}{r_p^4}}}\left(\frac{R-z}{R}\right)^{\frac{3}{2}}, \qquad (3)$$

where A_e is the peak spherical aberration, r_p the radius of the exit pupil and R the radius of the reference sphere. In the present case, according to our previous comments, we can suppose that our problem corresponds to an exit pupil centered at z=5.0 mm, with $A_e = 88.6\lambda$, $R = 395.0\ mm$ (since z=5.0 mm) and $r_p = 28.024\ mm$ (corresponding to $h_p = 28.0\ mm$).

In summary, for plotting caustics in the present case we have two possibilities: our numerical procedures for finding the turning point of $y(z;h)$ in (2), or expression (3), valid when only spherical aberration is present. The comparison between both methods will be done in a later Figure.

3. Calculation of the PSF by scalar diffraction theory

It is well known that ray tracing cannot be used for precise PSF calculations near the focal zones [2][3]. Conversely, as in our present case, scalar diffraction theory is very adequate for that purpose [4] [5]. In fact the procedures presented in these last references are very slow for our present application since they do not take profit of the full rotational symmetry present. Now, to use the Fourier-Bessel transform is probably the fastest choice [6][7]. The development of numerical procedures for calculating the Fourier-Bessel integral has received considerable attention in recent times [8][9]. Provided one has not a requirement for high speed, it is not necessary to use any of these special procedures and a check for no aliasing in the data is enough. There is only a subtle detail to be taken into account: when calculating the intensities corresponding to radial distances far from the optical axis, any small absolute error in this intensity may give rise to a large error in integrated energies, because of the radial symmetry. Thus, calculating the complex amplitudes (or intensities) with good precision with Fourier –Bessel procedures is not a major problem, whereas calculating the total energies extended to any plane perpendicular to the optical axis is difficult. It is important to note that, in our present case, the calculation of the isophotes will be precise enough to demonstrate our future claims.

As a first example, for a wide axial zone up to 30 mm away from the Gaussian plane, Fig. 3 shows the single isophote of intensity 0.004, being 1 the highest value present in the graph (not shown). It has been calculated for our optical system ($0 \leq h \leq 22.0$ mm) by, first, sending a number of rays (here 100) and fitting with respect to ρ the resulting points P_h . These define a curve like the dots in Fig. 2, but without the cusp, since z=5.0 mm (not z=250.0 mm as in that Figure). Subsequently, the calculation of complex amplitude propagation from a circular pupil situated at z=5.0 mm is done within scalar diffraction assumptions. Fig. 3 also shows the turning points (cusps of the figures equivalent to Fig. 2 for the different z) that define numerically the geometric caustic (dots) together with the corresponding analytic expression (3), plotted as a continuous curve.

As presented, Fig. 3 is not valid for quantitative evaluations, but illustrates several important issues. First, the caustic does not really correspond to a zone of high intensities of the field, but mostly to a limiting zone, since the relevant fact extracted from observation of the figure is that beyond the caustic there is almost no light. A second conclusion may also be immediately drawn: although not quantitative, the aspect of this isophote is enough to demonstrate that any plane (perpendicular to the axis) in the 370-385 mm zone will contain a lot of concentric rings, a phenomenon easily observed in the experiments. Moreover, in practice, these rings are the easiest way to determine the position z of the plane of any light detector (as a CCD camera). A third interesting observation is worth to mention: the striking coincidence between the crosses (the caustic computed numerically by searching for the cusps of Fig. 2 for each plane z) and the continuous curve plotted according to equation (3), even for z values lying quite far from the Gaussian image plane. This fact demonstrates that the numerical procedure being proposed is highly accurate.

The isophotes of Fig. 4 correspond only to the focal zone of our experiment (see the Z-axis values) and are scaled between 0 and 10000 for intensities. These units are arbitrary but it is important to mention that the scale we are implicitly defining here will remain fixed for all forthcoming figures. Fig. 4 further illustrates the fact that the caustic is not associated with a high intensity. In fact, it shows that near the focal zone the caustic has no physically clear significance. We also see that the highest intensity is around the 394.5 mm axial position, while the Gaussian image plane is at 400.0 mm. This last position is just the limit being plotted on the right of Fig. 3 and Fig. 4 and, of course, coincides with the apex of the caustic (the intersection with the optical axis). Note that, by taking any slice of the isophotes at any given value z, Fig. 4 contains all the information about any corresponding PSF of our system.

4. Self consistency of scalar diffraction calculations

The calculation of the diffraction integral using the scalar diffraction approach allows a quite arbitrary choice of the integration domain. Assume we consider two wavefronts of the same propagating wave, defined respectively by $C(z_1)$ and $C(z_2)$, with $z_2 > z_1$. We may calculate the complex amplitude at any specific focal region by propagating the respective wavefronts either from z_1 or from z_2 and the results have to be the same in both cases. This has to be certainly true provided that both wavefronts are mathematically well defined. According to what we have discussed in paragraph 2, what is needed for the integration process to be mathematically well defined, is that no point within the integration domain is reached by two different rays. For centered circular apertures, this is the same as stating that the aperture has to be limited by the heigth h_c, as defined above when describing Fig. 2. In fact, the complete explanation for the conditions for the validity of the integration domain is slightly more involved, and the limiting value mentioned has to be in fact $h_c(z_2)$, since h_c depends on z.

Thus, let us develop a detailed and complete analysis of our example. First it is clear that, within our computational scheme, all centered circular apertures defining the same cone of light in object space have to be considered equivalent. It is known that, strictly speaking, this is not true but the differences are usually negligible [5]. When we analyze the image space, i.e. once the light exits the lens, the conditions change according to the position of the plane z for the wavefront. These changes are better explained by analyzing Fig. 5, that corresponds to the incident cone of light defined by the circular aperture of radius $h_p = 22.0mm$.

The continuous curve in Fig. 5 is simply the outer sheet of the caustic, as computed using expression (3). Next let us consider, for each z, the maximum height that any incident ray may attain within the z plane; this is precisely the cusp or the maximum value of $y(z;h)$ in (3). This condition defines the dotted curve in Fig. 5. When $z \approx 0$ this height will be $\approx 22mm$, the height attained by the upper limiting ray. As we increase z the maximum of $y(z;h)$ in (3) decreases, defining the left side of the dotted curve, which is a straight line corresponding to the marginal ray in image space, since $h_c(z) = h_p$. As we further increase z (in the present example after $z \approx 260mm$) the maximum height attainable corresponds to $h_c(z) < h_p$ and the dotted curve tends to be a line tangent to the caustic, not being a straight line any more. This is to say that, for these bigger z values, the ray that attains the highest point within the plane is not the one entering the lens at the border, but some lower ray. The important conclusion from these comments is that, provided we keep $z < 260mm$ (the exact value is found by searching where the cusp of Fig. 2 starts to appear), any transversal cut of the light cone defined by $h_p = 22.0mm$ corresponds to a well defined wavefront. Besides that plane ($z > 260mm$), the optical path length is not a one-valued function in the integration domain so that the normal integration of functions is not possible.

In summary: self consistency in our developments implies that numerical integration within scalar diffraction approximation has to give rise to identical results whenever the integration domain corresponds to the same cone of light and $z < 260mm$. The next step is to confirm the validity of this result in our example. In essence, what we have to check is that for any two wavefronts of the same propagating wave, defined respectively by $C(z_1)$ and $C(z_2)$, with $z_2 > z_1$, calculating isophotes at any specific focal region by computing the Fourier-Bessel integral from with z_1 or from with z_2 give the same results in both cases. For example, z_1 can be at the exit of the lens (as $z_1 = 5.0mm$), and z_2 any other distance fulfilling the condition $z < 260mm$. An important point has to be mentioned here: while the wavefront immediately at the exit of the lens deviates from the sphere according to the well known 4th power factor of spherical aberration with high accuracy, the propagation of the wavefront up to $z_2 >> z_1$ gives rise to a much more involved dependence of the aberration on the radial distance ρ for the plane z_2. This fact poses no major problem for numerical integration by Fourier-Bessel, provided it is taken into account. Thus, the aberrated wavefronts calculated with the procedures introduced in paragraph 2 can always be fitted with arbitrarily high precission by using a polinomial expansion involving only even powers of the radial distance. In summary, the validity of one of the crucial ideas in our present developments has been tested in depth, leading to the following conclusion: provided one uses a good polynomial fit for the aberrated wavefronts (allowing a high degree polynomial for the fitting), the computation of isophotes by means of scalar diffraction integrals corresponding to different propagation distances shows a perfect coincidence. For example, Fig. 4 would be virtually repeated (thus not presented) when plotting the isophotes obtained by propagating the wavefront from a circle of radius $r_p = 12.0mm$ at the plane $z = 150.0mm$. Other interesting calculations will be illustrated in forthcoming Figures.

5. A significant experiment

Having the capability of calculating absolute values of the complex amplitudes with high precision can help to understand remarkable observations on the optical bench. One of these curious cases, that we have encountered while performing the present work is the following. The calculated isophotes in the focal zone corresponding to Fig. 4 are in fact similar to those calculated for a centered aperture 6.9 times smaller in area (this is, a radius of $22 \times 0.38 = 8.36mm$), as shown in Fig. 6. This Figure shows that, not only the isophotes are quite similar near focus ($z = 393 \leftrightarrow 396mm$) but, indeed, the intensity attains higher values now than before (the level 9000 isophote is wider now than in Fig. 4).

The explanation is clear: since our optical system becomes highly aberrated as the aperture increases, the contribution of these highly aberrated zones leads (mostly) only to an increase of the background light. It is pertinent here to remind our previous comment on the precision of the calculations of complex amplitudes and energies: the intensities are higher in the focal zone with smaller aperture because the additional energy entering the system at higher aperture gives only slightly higher intensities far from the axis. Clearly, when speaking about PSFs this implies that more aperture is giving worse PSF even in terms of effective image brightness.

Although there are no contradictions in these explanations, since the above observation can certainly be considered an interesting phenomenon, we decided to perform a more detailed study and an experimental test. In effect, an additional and complementary explanation for the fact of having more intensity with less aperture can easily be obtained in terms of phasors [10][11]. By calculating the complex amplitude on the axial position $z = 393.6mm$ using the phasor representation we obtain the plot presented in Fig. 7.

This Figure represents the increase of the complex amplitude (at the cited axial point) as one increases the radius of the centered aperture up to our limiting value. The figure begins at (0,0) and shows first a quick increase in modulus as the radius increases, since the cross in the figure corresponds to $r_p = 7.0mm$ and the circle to $r_p = 8.4mm$. This last radius corresponds (approx.) to the one of Fig. 6 and we see that virtually gives the maximum intensity (the intensity is simply the square of the amplitude represented here as the distance to the origin). Besides, when the radius further increases the amplitude curls faster and faster. The maximum amplitude in Fig. 7 has a modulus of about 100 of our arbitrary units, which corresponds to the maximum intensity of 10000 mentioned for Fig. 4. Note that a phasor representation near the axial position $z = 394.5mm$ would give a higher maximum amplitude, according to the previous comment about Fig. 4. A similar behavior in terms of phasors could be shown for different calculation points and that kind of computation fully explains our phenomena. The final test (experimental) of these predicted observations is presented in Fig. 8, that shows the measured intensities at the plane $z = 393.6mm$, corresponding to the three radius $r_p = 7.0, 8.4, 22.0mm$. We have used a CCD digital camera with pixel size of 4.65 microns. The PSFs look very similar and their profiles agree with the calculations. Although absolute intensity measurements are difficult with a CCD camera, we have carefully checked in our optical bench that the three axial intensities are indeed increasing in the order predicted by Fig. 7: $r_p = 7.0, 22.0, 8.4mm$, leaving no doubt on the accuracy of our calculations.

6. Summary and conclusions

On the basis of standard ray tracing, we have presented procedures for the numerical calculation of wavefronts and caustics in optical systems. By combining these procedures with the propagation integrals of diffraction theory, methods for calculating the corresponding PSFs within the scalar diffraction approximation (under Fourier-Bessel conditions) have also been developed.

A list of the main results developed in the work is the following:

- a numerical procedure for determining wavefronts and caustics.
- a comparison between these numerical procedures and analytical formulae, when available, together with a discussion of the physical significance of the caustic near and far from the focal zone.
- a way for calculating the PSFs (using the integral formula that propagates the wavefront) for a wide range of distances between the pupil and the calculation plane within the scalar diffraction theory; the capabilities, limitations and self-consistency due to the very definition of that integral are discussed.
- a detailed analysis of a remarkable example regarding a standard lens, its aberrations and performances, together with an experiment which demonstrates the accuracy of our procedures.

Acknowledgements

Most of the presented work was done during the stay of the author in the Optical Sciences Center in Tucson, Arizona (June-September 2009), funded through a grant from 'Programa de Movilidad de Profesores e Investigadores' of the Spanish 'Ministerio de Educación y Ciencia'. The author also thanks this Institution for the funding of the Research Project DPI2008-04175DPI.

References

1. W.T. Welford, *Aberrations of Optical Systems* (Adam Hilger, Bristol 1986).
2. W.J. Smith, *Modern Optical Engineering* (McGraw-Hill, New York, 2000).
3. V.N. Mahajan, *Optical Imaging and Aberrations, Part II* (SPIE Press, Bellingham, 1998), Chap. 1.
4. S. Bosch, and J. Ferré-Borrull, "Analysis of waves near focus: Method and experimental test," Appl. Phys. Lett. 80, 1686-1688 (2002)
5. J. Ferré-Borrull, and S. Bosch, "Formal description of diffraction in optical systems: calculations and experimental evidence," Appl. Phys. Lett. 85, 2718-2720 (2004)
6. J.W. Goodman, *Introduction to Fourier Optics* (McGraw-Hill, New York, 1968).
7. A.E. Siegman, "Quasi fast Hankel transform," Opt. Lett. 1, 13-15 (1977).
8. Li Yu, et. al., "Quasi-discrete Hankel transform," Opt. Lett. 23, 409-411 (1998).
9. M. Guizar-Sicairos, and J.C. Gutiérrez-Vega, "Computation of quasi-discrete Hankel transforms of integer order for propagating optical wave fields," J. Opt. Soc. Am. A 21, 53-58 (2004).
10. E. Hecht, *Optics* (Addison-Wesley, New York, 2002), Chap. 7.
11. S. Bosch, and J. Ferré-Borrull, "The focal shift in converging of waves" J. Mod. Opt. 50, 2221-2229 (2004)

figure captions

Fig. 1. Layout of our optical system: illustrating the procedure for finding the wavefront corresponding to a distance z.

Fig. 2. Obtaining the wavefront for $z = 250.0\ mm$ with $\Delta h = 0.28\ mm$. The continuous line is the reference sphere.

Fig. 3. Isophote of 0.004 relative intensity corresponding to a wide zone around the focus. The analytic caustic (line) and the numerically computed caustic (dots) are also shown.

Fig. 4. Isophotes near the focal zone of our optical system. The maximum intensity is 10000. The analytic caustic (line) and the numerically computed caustic (dots) are also shown.

Fig. 5. Continuous line: caustic computed using expression (3) from text. Dots: maximum height attained by any incident ray for the different planes Z.

Fig. 6. Isophotes near the focal zone of our optical system when the aperture radius is 4/10 of the one used for Fig. 4.

Fig. 7. Phasor construction corresponding to the axial position $z = 393.6mm$. The cross corresponds to pupil radius $r_p = 7.0mm$ and the circle to $r_p = 8.4mm$

Fig. 8. Intensities at $z = 393.6mm$ for $r_p = 7.0, 8.4, 22\ mm$ (from left to right).

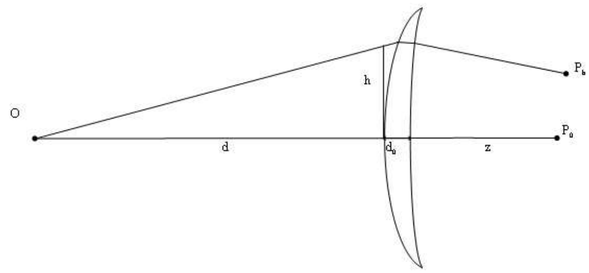

254x190mm (96 x 96 DPI)

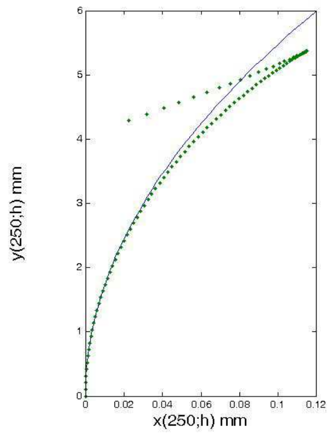

451x213mm (72 x 72 DPI)

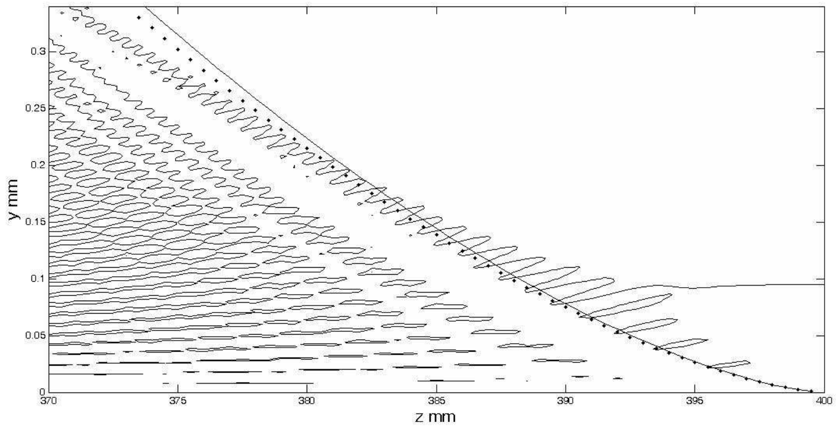

451x214mm (72 x 72 DPI)

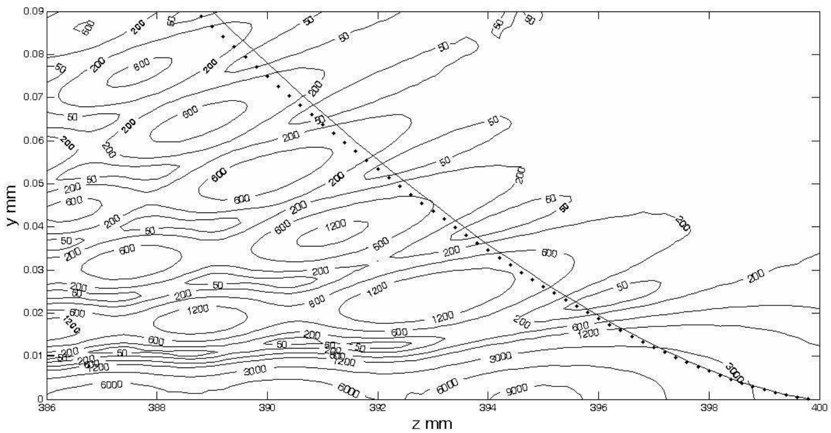

451x215mm (72 x 72 DPI)

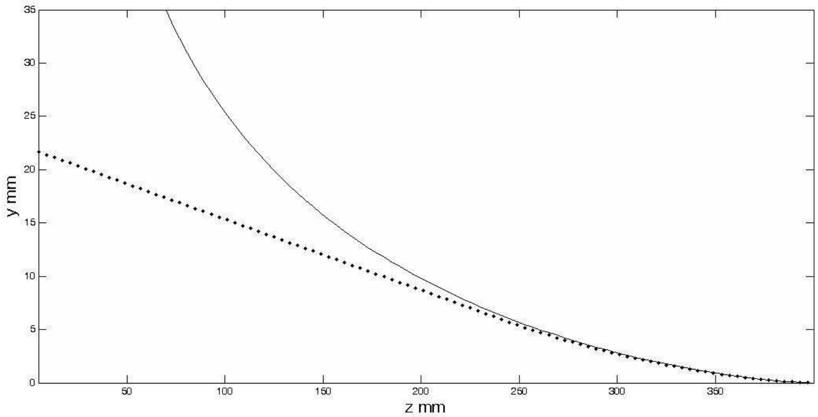

451x207mm (72 x 72 DPI)

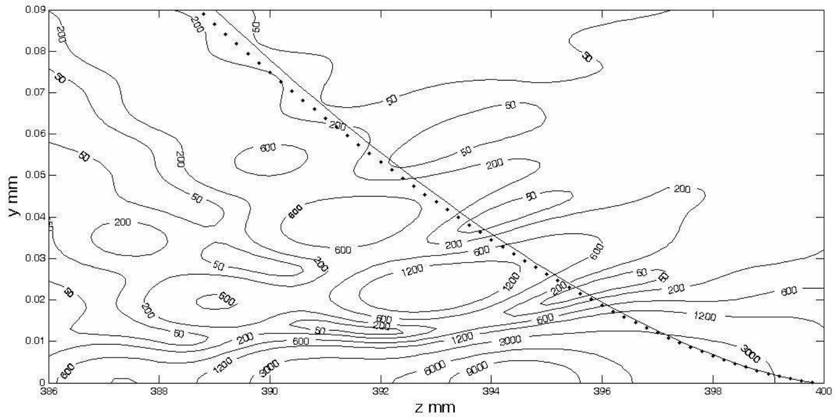

451x207mm (72 x 72 DPI)

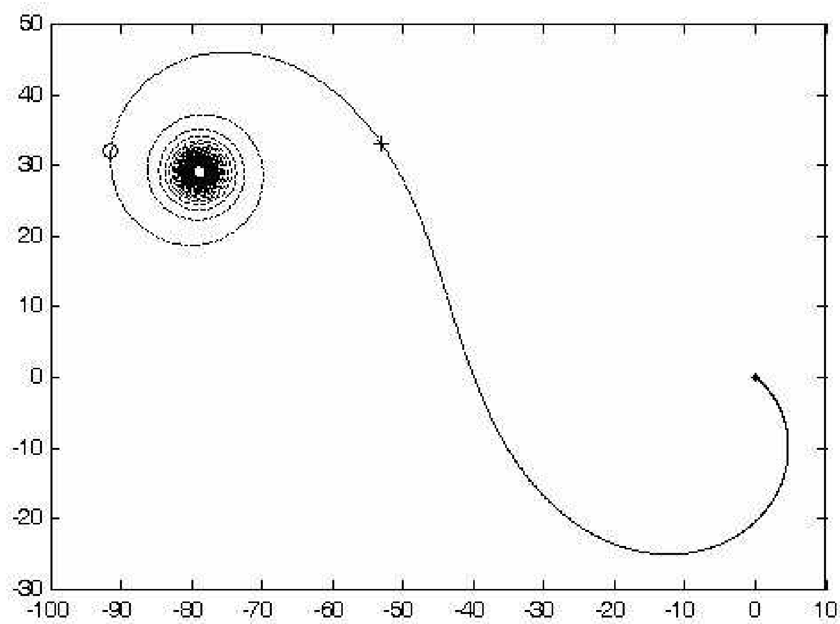

197x148mm (72 x 72 DPI)

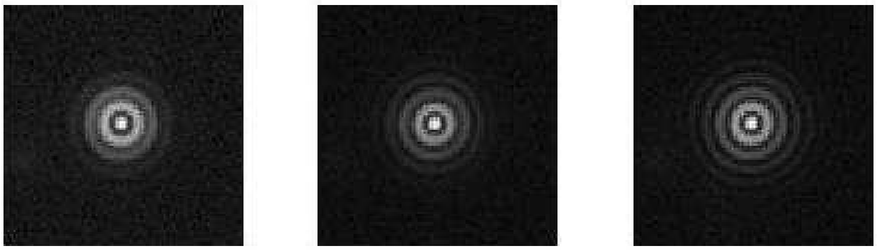

119x35mm (96 x 96 DPI)